

PAPER

Characterization of carrier transport behavior of specific type dislocations in GaN by light assisted KPFM

To cite this article: Cuihong Kai *et al* 2020 *J. Phys. D: Appl. Phys.* **53** 235104

View the [article online](#) for updates and enhancements.




IOP | ebooks™

Bringing together innovative digital publishing with leading authors from the global scientific community.

Start exploring the collection—download the first chapter of every title for free.

Characterization of carrier transport behavior of specific type dislocations in GaN by light assisted KPFM

Cuihong Kai^{1,2}, Xiaojuan Sun^{1,2}, Yuping Jia^{1,2}, Ke Jiang^{1,2}, Zhiming Shi^{1,2}, Jianwei Ben^{1,2}, You Wu^{1,2}, Yong Wang^{1,2} and Dabing Li^{1,2,3} 

¹ State Key Laboratory of Luminescence and Applications, Changchun Institute of Optics, Fine Mechanics and Physics, Chinese Academy of Sciences, Changchun 130033, People's Republic of China.

² Center of Materials Science and Optoelectronics Engineering, University of Chinese Academy of Sciences, Beijing 100049, People's Republic of China

E-mail: lidb@ciomp.ac.cn and sunxj@ciomp.ac.cn

Received 8 October 2019, revised 19 January 2020

Accepted for publication 11 February 2020

Published 3 April 2020



Abstract

The direct characterization of carrier transport behavior at different types of dislocations in GaN is still questionable due to the current lack of feasible strategy. Herein, we developed a method by combining ultraviolet light-assisted Kelvin probe force microscope with defect selective etching technology. The dislocation types could be confirmed by the shape of the etching pit, and the photogenerated carrier recombination behavior at specific dislocation. Thus, it can be characterized by ultraviolet light-assisted Kelvin probe force microscope, which paves the way for analysis of carrier transport behavior at different types of dislocations in GaN. The screw dislocations are found to be the main non-radiative recombination centers, and mainly responsible for leakage current in GaN based device. This shows higher surface potential and higher electron concentration due to the donor defects introduced during dislocation growth. Conversely, a barrier is generated around the edge and mixed dislocations, which could suppress the non-radiative recombination at the dislocation. The present work provides a feasible way to direct characterization of specific type dislocations in GaN. Moreover, this method can be used to characterize other III-nitride materials.

Keywords: dislocation, KPFM, carrier transport

(Some figures may appear in colour only in the online journal)

1. Introduction

III nitride semiconductors are promising materials for ultraviolet (UV) photoelectronic and power devices due to their wide band gap, high thermal conductivity, and high electron mobility [1–3]. Due to the lattice mismatch and thermal mismatch between the heterogeneous substrate and the epitaxial layer, it is inevitable the high density dislocations exist in GaN-based materials. In order to optimize the performance of GaN-based devices with long-life and high-reliability, it is necessary to understand the influence of dislocations on the optical and electrical performance of III nitride materials. However,

it is difficult to know enough information about the dislocation type and optoelectronic property of a single dislocation simultaneously due to the limitation of characterization technique. Over the last 30 years, significant efforts have been dedicated to obtaining the photoelectric performance of a specific dislocation. The cathodoluminescence (CL) combined with transmission electron microscopy (TEM) provide a nanoscale characterization of luminescence response around dislocation, and give the conclusion that the dislocation is non-radiative recombination center [4]. Transmission electron microscopy (TEM) and electron beam induced current microscopy (EBIC) were used to determine the electrical activity of threading dislocation, the results show that the threading dislocation is recombination centers [5]. Hamachi *et al* used conductive

³ Author to whom any correspondence should be addressed.

atomic force microscopy (C-AFM) to characterize the local current of GaN single crystal. The leakage current and lower effective Schottky barrier heights at threading dislocations could be observed [6]. Yamaoka *et al* used C-AFM and aqueous potassium hydroxide solution etching to investigate the origin of vertical leakage current in AlGaIn/GaN high-electron mobility transistors (HEMTs) [7]. The results indicate that screw-type threading dislocations in AlN nucleation layers create the vertical leakage current path in HEMT structures [8]. Based on the analysis of the relationship between the properties of nitride materials and the dislocation concentration, it is concluded that dislocations are non-radiative recombination centers and scattering centers [9, 10]. The result that screw dislocations are the main leakage centers is obtained based on the analysis of the relationship between device performance and dislocation density [11, 12]. However, there are few literatures that discuss the relationship between different types of dislocations and the optoelectronic properties of materials. Yamamoto *et al* combined TEM with CL to characterize optical properties of dislocations in GaN. They found that the edge dislocation parallel to the *c* plane was very active, while the screw dislocation is less active [13]. Albrecht *et al* used CL and defect selective etching to study specific dislocation, giving the result that the recombination strength of the *a*- and (*a* + *c*)-type dislocations is influenced by impurity gettering, while the *c*-type screw dislocation is not recombination active [14]. Naresh-Kumar *et al* combined two scanning electron microscopy techniques to investigate the influence of dislocations on the light emission from Si-doped *c*-plane GaN, and confirmed that both pure edge dislocations and those with a screw component act as nonradiative recombination centers [15]. Until now, the direct observation and characterization of physical properties and carrier transport mechanisms of the three types of dislocations in III-nitride semiconductor materials still need to be further explored.

Kelvin probe force microscope (KPFM) is a method for characterizing localized surface potential. By characterizing the surface potential of the sample under steady-state and excited-state, information such as doping type [16], polarity [17], carrier transport [18], carrier recombination velocity at defect [19, 20] and local charge trapping [21] could be acquired. However, the KPFM cannot resolve the type of dislocations. Lu *et al* enlarged the dislocation by nanoindentation, and calculated the minority diffusion lengths, carrier recombination velocities based on the results of light assisted KPFM [19]. However, this method cannot distinguish the dislocation type of a single dislocation and realize the carrier transport characterization of a special dislocation. To acquire carrier transport information of specific type dislocation, it is necessary to realize observation and characterization of single dislocation. In this regard, post-process treatment to enlarge the dislocation would be a good choice to solve aforementioned problem. Based on the shape of the etch pit, the type of dislocation could be distinguished [22–24]. In this work, we combine UV-assisted KPFM with defect-selective etching technology to characterize the carrier transport behavior at different type dislocations in GaN, and the effect of different type dislocations on the properties of GaN is discussed.

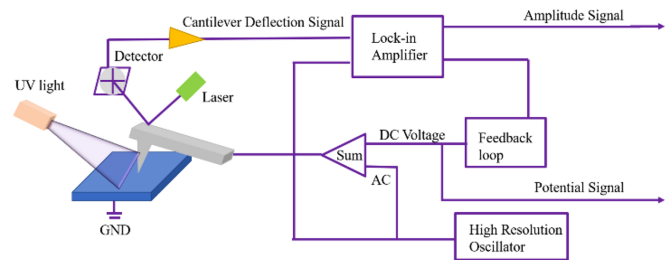


Figure 1. The schematic principle of UV-assisted KPFM. The UV light is illumination on the top surface of sample.

2. Experimental methods

The GaN sample was obtained by metalorganic chemical vapor deposition (MOCVD) on sapphire. Ammonia (NH₃) and trimethylgallium (TMG) were used as N and Ga precursors, respectively. A 20 nm thick GaN buffer layer was initially-grown on a *c*-plane sapphire substrate at 635 °C. Then, an undoped 5-μm thick GaN template was grown at 1050 °C. The full width at half maximum (FWHM) of (002) and (102) planes acquired by x-ray rocking curve (XRC) are 252 and 320 arcsec, respectively. The densities of dislocations with a screw and edge components calculated from the XRC-FWHM value are $1.27 \times 10^8 \text{ cm}^{-2}$ and $5.43 \times 10^8 \text{ cm}^{-2}$, respectively [25, 26]. The n-type carrier concentration of GaN obtained by the Hall is $1.98 \times 10^{17} \text{ cm}^{-3}$. The as-prepared sample was etched in H₃PO₄ (85%) at 190 °C for 100 min using a poly-tetra fluoroethylene reactor.

The KPFM (Bruker MultiMode-8 surface potential mode) was used to characterize the surface potential. The MESP model tip with a reflective CoCr backside coating was used. The radius of tip was 35 nm. The wavelength and power of light is 340 nm and 100 mW, respectively. Figure 1 is the schematic principle of UV-assisted KPFM. The UV light is illumination on the top surface of sample. The detailed description of light-assisted KPFM is described in our previous work [27]. The scanner model of AFM and KPFM was AS-130VLR ('J' vertical). The CL measurements were performed at an accelerating voltage of 10 kV.

3. Results and discussion

Figure 2 is the AFM morphology of uGaN after etching. The three graphs are the section profiles along the white lines crossing the etch pit. As shown in the graphs, three kinds of morphologies could be observed: inversed truncated hexagonal shape, inversed hexagonal pyramid shape, and a combination of inversed truncated hexagonal and inversed hexagonal pyramid shape, corresponding to screw dislocation, edge dislocation, and mixed dislocation, respectively [28].

Figures 3(a) and (b) are surface potential images of the same area in figure 2 acquired in the dark and under UV irradiation, respectively. The line scan of surface potentials along the lines in figures 3(a) and (b) are shown in figures 3(c)–(e). It can be observed that the surface potential of screw dislocation

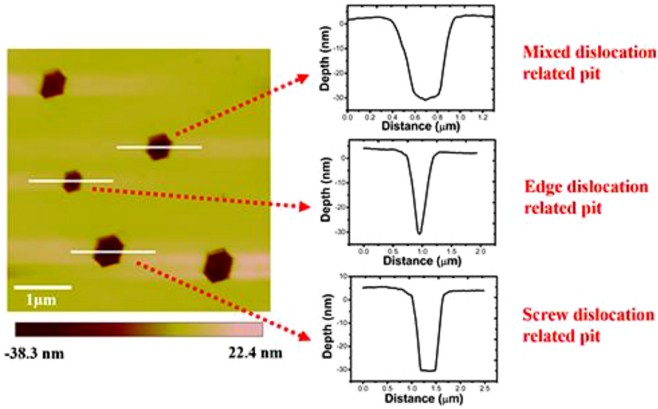


Figure 2. The morphology of uGaN after etching measured by AFM (left) and the section profiles along the white lines indicated in AFM image (right).

is higher than that of planar surface, while the surface potential of edge and mixed dislocations are lower than that of planar surface in dark.

The relationship of the surface potential (V_{DC}) and work functions of the sample (ϕ_{sample}) and the tip (ϕ_{tip}) can be written as [27]:

$$V_{DC} = V_{sample} - V_{tip} = (\phi_{tip} - \phi_{sample}) / e \quad (1)$$

where $\phi_{sample} = \chi + (E_c - E_f)$. V_{sample} and V_{tip} are the surface potentials of the sample and the tip. χ is the electronic affinity. E_c and E_f are the energy at conduction band bottom and Fermi level. According to equation (1), the smaller V_{DC} corresponds to a lower E_f , i.e. a low electron concentration. In the dark, the higher surface potential at screw dislocation indicates a higher electron concentration gathered at it. For edge and mixed dislocations, the potential is lower than that at planar surface, indicating the electron concentration at these dislocations are lower than that at planar surface. Based on electrical neutral conditions, the electron concentration of GaN can be written as:

$$n_0 = \sum_j N_D - \sum_i N_A, \quad (2)$$

where $\sum_j N_D$ and $\sum_i N_A$ represent the total concentration of j kind donor and i kind acceptor impurities, respectively. It is assumed that both donors and acceptors are ionized.

According to above analysis, the electron concentration at screw dislocation is higher than that at planar surface, while that at edge and mixed dislocations is lower than that at planar surface. Combined with equation (2), it can be inferred that screw dislocations introduce a large number of donor defects, while edge and mixed dislocations introduce more acceptor defects. The density-functional calculation show that edge dislocation is likely to trap gallium vacancies, oxygen, and gallium vacancy-oxygen defect complexes [29], while a Ga-filled core screw dislocation could yield shallow gap states at 0.2 eV below the conduction band minimum [30]. Arslan *et al* also observed a large amount of oxygen (O) impurities around the screw dislocation [31]. Therefore, a large number of acceptor-type Ga vacancy complex defects at edge

dislocations may be the main reason of the decrease in electron concentration, and the donor type O impurities may be the main reason for the increase in electron concentration at screw dislocation.

Under UV light irradiation, as shown in figures 3(c)–(e), compared with the surface potential in the dark, the potential of screw dislocation is increased by 34 mV, while that of the nearby planar surface near increased by 54 mV. According to our previous work, the greater this potential difference is, the lower the carrier recombination rate [20]. The surface potential results show a ± 5 mV fluctuation. Therefore, it can be concluded that the carrier recombination rate at screw dislocation is faster than that at planar surface (to improve the accuracy of the results, the planar surface is taken near the dislocation and on the same horizontal line as the center of dislocation). The surface potential of the edge dislocation and the nearby planar surface are increased by 47 mV and 54 mV, respectively. For mixed dislocation, the potential increases by 67 mV at it and 70 mV at the nearby planar surface. This indicates that the carrier recombination rate at edge and mixed dislocations are similar with that at planar surface. Carrier recombination includes radiative and non-radiative recombination. Although the results of KPFM cannot distinguish the recombination type. Dislocations in GaN are non-radiative recombination centers have been reported by previous works [14, 32, 33]. Therefore, it is considered that the carrier recombination rate at dislocations discussed above are mainly non-radiative recombination rate.

To verify this point, CL was performed at the center of three type pits as shown in figure 4. Since the diameter of the pit is 600–800 nm and the depth of pit is about 30–35 nm, the effect of the etch pits of different sizes on the light extraction efficiency is very weak when the center of the dislocation is irradiated with an electron beam with a diameter of 100 nm. Massabau *et al* has discussed the effect of the pit geometry on the CL properties and given the results that the difference in light extraction efficiency between the V-pit and its surroundings can be ignored [34]. It can be observed that the illuminating intensity at the dislocation is significantly lower than the planar surface, which proves that all three dislocations are non-radiative recombination centers. Except the planar surface, edge dislocation exhibits the strongest band edge emission intensity, and that of screw dislocation is the weakest. This indicates that screw dislocation has the largest non-radiative recombination rate and edge dislocation has the smallest non-radiative recombination rate in the three types of dislocations, which is consistent with the results obtained by the surface potential.

To further understand the effect of dislocations on carrier recombination, the mechanism is schematically expressed in figure 5. The screw dislocation aggregates electrons. Based on the relationship $n_0 \times p_0 = n_i^2$, the hole concentration at screw dislocation is lower than that at perfect crystal. The Fermi level will be raised and a potential well will be formed at the dislocation, as shown in figure 5(a). Under UV light, the photogenerated holes diffuse into dislocation driven by the hole concentration gradient. The non-radiative recombination at screw dislocation is promoted. Edge dislocation has gathered holes.

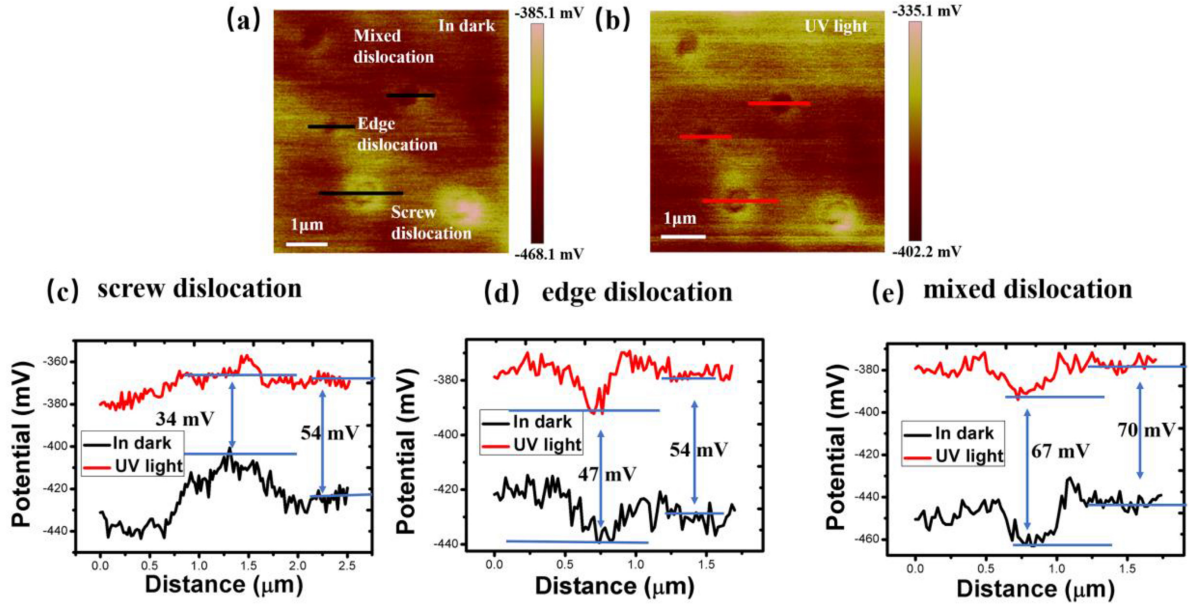


Figure 3. (a), (b) Surface potential in the dark and under UV light obtained by KPFM. (c)–(e) Section profiles along the black lines (in dark) and red lines (UV light) crossing etch pits.

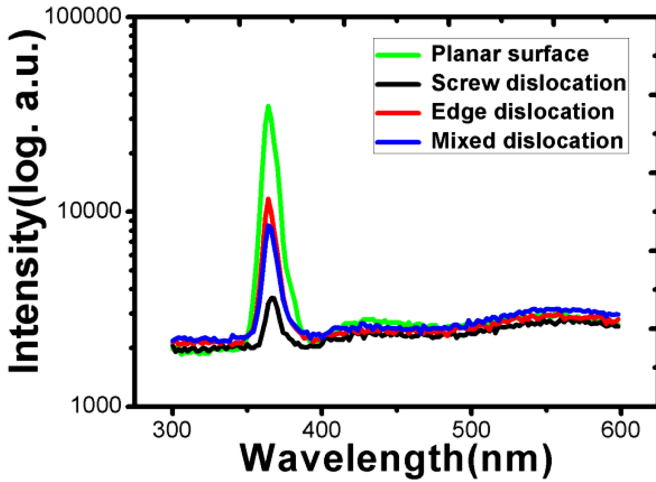


Figure 4. The cathodoluminescence spectrum at different dislocations. The black, blue, red, and green curves are the spectra at screw dislocation, edge dislocation, mixed dislocation and planar surface, respectively.

The Fermi level is reduced and a barrier is formed at edge dislocation, as shown in figure 5(b). Under UV light, the photo-generated holes diffuse to edge dislocation is inhibited. Therefore, the nonradiative recombination at it is suppressed. Carrier transport behavior at mixed dislocation is similar to that at edge dislocation. However, due to the screw dislocation component in mixed dislocation, the band edge emission intensity at the mixed dislocation is lower than that at the edge dislocation.

The effect of different type dislocations on Schottky barrier current is further discussed. Based on the thermal electron emission model and the tunneling model, the Schottky barrier current density (j) from semiconductor to metal can be expressed by the following equation.

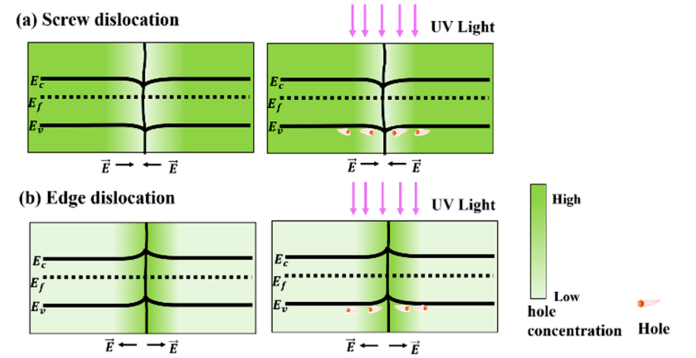


Figure 5. The schematic diagram of the carrier transport and the equilibrium energy band at (a) screw dislocation; (b) edge dislocation.

$$j = j_e + j_t = A^* T^2 \exp\left(-\frac{\phi_m}{k_B T}\right) \left(\exp\left(\frac{eV}{k_B T}\right) - 1 \right) + A^* T^2 / k_B T \int_{E_{fm}}^{q\phi_m} F_s T(E) (1 - F_m) dE \quad (3)$$

where j_e and j_t are the peak emission current density and tunneling current density. A^* , T , k_B , e and V are the effective Richardson constant, temperature, Boltzmann constant, electron charge and bias, respectively. F_s and F_m is the Fermi–Dirac distribution function of semiconductor and metal. $T(E)$ is the tunneling probability, which is inverse proportion to the height and thickness of the barrier. ϕ_m is the Schottky barrier, which can be affected by interface state and image force. Since the present work discusses the effect of dislocations on the Schottky barrier in the same sample, the effect of surface states on the barrier could be ignored.

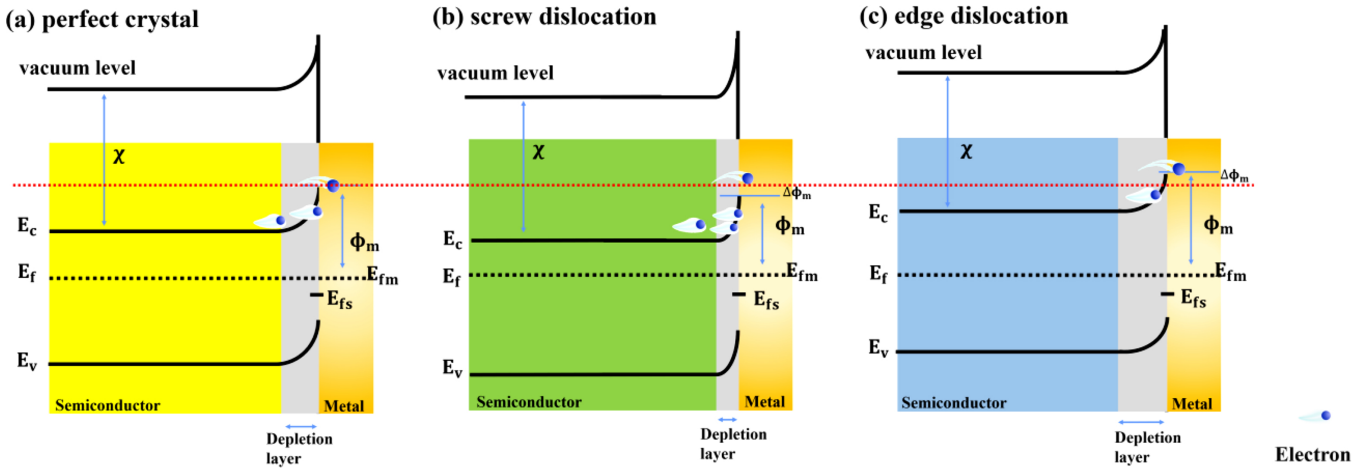


Figure 6. The schematic diagram of energy band at (a) perfect crystal, (b) screw dislocation, (c) edge dislocation. The E_{fm} is the Fermi level of contact electrode. The E_{fs} is the surface Fermi level.

The GaN, which is grown on sapphire, is affected by compressive stress, resulting in the energy band broadening. Stress release at dislocations in GaN reduces the band broadening. Since the stress relaxation of the dislocations has been completed after GaN growth, the effect of the charge accumulation by the dislocation on the Schottky current is discussed here. The schematic diagrams of the Schottky barrier and electron transport at dislocation and perfect crystal are shown in figure 6 to discuss the influence of dislocations on Schottky contact. Compared with perfect crystal, the screw dislocations introduce a large number of electrons. When the Schottky contact formed, the mirror force at screw dislocation is larger than that at the perfect crystal. The Schottky barrier height and thickness at dislocation is reduced compared with that at perfect crystal, which is attributed to the larger mirror force and higher electron concentration at dislocation, as shown in figure 6(b). As a result, the tunneling probability $T(E)$ at screw dislocation is increased. According to equation (3), The j_e and j_t are increased compared with that at perfect crystal. The edge dislocations introduce more acceptor-type defects, which could reduce the electron concentration. When the Schottky contact has formed at edge dislocation, the mirror force is smaller compared with that at perfect crystal due to the smaller electron concentration at the dislocation. Then, the Schottky barrier height and thickness at edge dislocation will be increased, as shown in figure 6(c). Thus, compared with that at perfect crystal, $T(E)$ at edge dislocation is decreased, and the j_e and j_t are decreased. Based on above discussion, one can obtain the following conclusion: for GaN-based MSM UV detectors, screw dislocations increase the dark current; the edge dislocations have an inhibitory effect on the dark current, but it reduces the photocurrent. This phenomenon was also observed in GaN MSM photodetector in our previous work [35].

According to above experiments and discussion, the decrease in dislocation density, especially the screw dislocation density, could effectively improve the luminous efficiency of GaN-based LED. While for GaN-based MSM photodetector, inspite of the strong non-radiative recombination

effect of screw dislocations, the large amount of donor impurities introduced by screw dislocations result in a larger built-in electric field when forming Schottky contacts, which will weaken the composite current caused by the screw dislocation. Therefore, the influence of the screw dislocation on the photocurrent is not obvious.

4. Conclusion

In summary, the effect of different type dislocations on photoelectric properties of GaN is studied by UV-assisted KPFM combined with defect selective etching, which allows the information acquirement of dislocation type and optoelectrical behavior of a single dislocation simultaneously. The screw dislocations are found to be the main non-radiative recombination centers, and are mainly responsible for leakage current in GaN based device, which shows greater surface potential and a greater electron concentration due to the donor defects introduced during dislocation growth. Conversely, the edge and mixed dislocation can aggregate holes due to the acceptor-type defects incorporated during its growth. A potential barrier is generated, which will block photo-generated holes from injecting to the dislocations and suppressing non-radiative recombination at the dislocations. The present work provides a feasible way to direct characterization of specific types of dislocations.

Acknowledgments

This work was supported by the National Key R&D Program of China (2016YFB0400101), National Science Fund for Distinguished Young Scholars (61725403), National Natural Science Foundation of China (61574142, 61874118, 61827813, 61704171), Key Program of the International Partnership Program of CAS (181722KYSB20160015), Jilin Provincial Science & Technology Department (20180201026GX), Youth Innovation Promotion Association of CAS.

ORCID iD

Dabing Li  <https://orcid.org/0000-0001-5353-1460>

References

- [1] Li D, Jiang K, Sun X J and Guo C L 2018 *Adv. Opt. Photonics* **10** 43
- [2] Sun Y et al 2018 *Light Sci. Appl.* **7** 13
- [3] Matioli E, Brinkley S, Kelchner K M, Hu Y L, Nakamura S, DenBaars S, Speck J and Weisbuch C 2012 *Light Sci. Appl.* **1** e22
- [4] Sugahara T, Sato H, Hao M, Naoi Y, Kurai S, Tottori S, Yamashita K, Nishino K, Romano L T and Sakai S 1998 *Japan. J. Appl. Phys.* **37** 398
- [5] Brazel E G, Chin M A and Narayanamurti V 1999 *Appl. Phys. Lett.* **74** 2367
- [6] Hamachi T, Takeuchi S, Tohei T, Imanishi M, Imade M, Mori Y and Sakai A 2018 *J. Appl. Phys.* **123** 161417
- [7] Hamachi T, Tohei T, Imanishi M, Mori Y and Sakai A 2019 *Japan. J. Appl. Phys.* **58** 050918
- [8] Yamaoka Y, Ubukata A, Yano Y, Tabuchi T, Matsumoto K and Egawa T 2019 *Semicond. Sci. Technol.* **34** 035015
- [9] Zhao D G, Yang H, Zhu J J, Jiang D S, Liu Z S, Zhang S M, Wang Y T and Liang J W 2006 *Appl. Phys. Lett.* **89** 112106
- [10] Arslan E, Altındal S, Özçelik S and Ozbay E 2009 *J. Appl. Phys.* **105** 023705
- [11] Lee S W et al 2006 *Appl. Phys. Lett.* **89** 132117
- [12] Usami S et al 2018 *Appl. Phys. Lett.* **112** 182106
- [13] Yamamoto N, Itoh H, Grillo V, Chichibu S F, Keller S, Speck J S, DenBaars S P, Mishra U K, Nakamura S and Salviati G 2003 *J. Appl. Phys.* **94** 4315
- [14] Albrecht M, Weyher J L, Lucznik B, Grzegory I and Porowski S 2008 *Appl. Phys. Lett.* **92** 231909
- [15] Naresh-Kumar G et al 2014 *Microsc. Microanal.* **20** 55
- [16] Wang R, Wang S N, Zhang D D, Li Z J, Fang Y and Qiu X H 2010 *ACS Nano* **5** 408
- [17] Wei J D, Neumann R, Wang X, Li S F, Fündling S, Merzsch S, Al-Suleiman M A M, Sökmen Ü, Wehmann H and Waag A 2011 *Phys. Status Solidi c* **8** 2157
- [18] Lan F and Li G Y 2013 *Nano Lett.* **13** 2086
- [19] Liu Z H, Xu K, Fan Y M, Xu G Z, Huang Z L, Zhong H J, Wang J F and Yang H 2012 *Appl. Phys. Lett.* **101** 252107
- [20] Kai C H et al 2019 *Sci. China Phys. Mech. Astron.* **62** 067311
- [21] Kondratenko S V, Lysenkob V S, Kozyrevc Y N, Kratzerd M, Storozhuka D P, Iliasha S A, Czibulad C and Teichertd C 2016 *Appl. Surf. Sci.* **389** 783
- [22] Hino T, Tomiya S, Miyajima T, Yanashima K, Hashimoto S and Ikeda M 2000 *Appl. Phys. Lett.* **76** 3421
- [23] Oliver R A, Kappers M J, Sumner J, Datta R and Humphreys C J 2006 *J. Cryst. Growth* **289** 506
- [24] Sang L et al 2017 *Appl. Phys. Lett.* **111** 122102
- [25] Zhang J C, Zhao D G, Wang J F, Wang Y T, Chena J, Liua J P and Yang H 2004 *J. Cryst. Growth* **268** 24
- [26] Moram M A and Vickers M E 2009 *Rep. Prog. Phys.* **72** 036502
- [27] Li D B, Sun X J, Jia Y P, Stockman M I, Paudel H P, Song H, Jiang H and Li Z M 2017 *Light Sci. Appl.* **6** e17038
- [28] Lu L et al 2008 *J. Appl. Phys.* **104** 123525
- [29] Elsner J, Jones R, Heggie M I, Sitch P K, Haugk M, Frauenheim T, Öberg S and Briddon P R 1998 *Phys. Rev. B* **58** 12571
- [30] Elsner J, Elsner J, Sitch P K, Porezag V D, Elstner M, Frauenheim T, Heggie M I, Öberg S and Briddon P R 1997 *Phys. Rev. Lett.* **79** 3672
- [31] Arslan I and Browning N D 2003 *Phys. Rev. Lett.* **91** 165501
- [32] Pauc N, Phillips M R, Aimez V and Drouin D 2006 *Appl. Phys. Lett.* **89** 161905
- [33] Gaubas E et al 2017 *Semicond. Sci. Technol.* **32** 125014
- [34] Massabau F C-P et al 2019 *J. Appl. Phys.* **125** 165701
- [35] Li D B, Sun X J, Song H, Li Z M, Chen Y R, Miao G Q and Jiang H 2011 *Appl. Phys. Lett.* **98** 011108